Self-Interference Flow of an Isotactic Polypropylene Melt in a Cavity during Injection Molding. II. Morphology and Crystallinity

Wenli Dai, Pengsheng Lui, Xiayu Wang

College of Chemistry, Xiangtan University, Hunan 411105, China

Received 30 January 2002; accepted 3 September 2002

ABSTRACT: This article is principally concerned with the morphology and crystallinity of isotactic polypropylene (iPP) parts molded by injection molding, during which a self-interference flow (SIF) occurs for the melt in the cavity. Scanning electron microscopy shows that a transverse flow takes place in SIF samples. Wide-angle X-ray diffraction and differential scanning calorimetry show that SIF moldings exhibit a γ phase, in addition to α and β phases, and high crystallinity. Meanwhile, the results for iPP moldings made by the conventional flow process, that is, conventional injection molding, are reported for comparison. © 2003 Wiley Periodicals, Inc. J Appl Polym Sci 88: 2791–2796, 2003

Key words: isotactic polypropylene (iPP); injection molding; morphology

INTRODUCTION

The first article of this series reports the melt self-interference flow (SIF) generated by a twin gate in a cavity during injection molding and discusses its effect on the mechanical properties, the thickness distribution, and the relationship of these properties to the processing conditions applied.[1] This article concentrates on the morphology of the isotactic polypropylene (iPP) parts molded in the presence of the interference flow.

Conventional injection-molded iPP displays a typical skin–core morphology. Kantz and coworkers[2,3] reported that three distinct layers could be identified: a nonspherulitic skin with a high degree of orientation of the molecular chains, a shear zone of oriented row structures, and a spherulitic core with no preferred orientation. With respect to the microstructure of conventional injection-molded semicrystalline polymers, Katti and Schultz[4] gave a good review. Fujiyama and Wakino[5] stated that in the skin layer, lamellae are perpendicular and parallel to the injection direction and that there exist crystallites with a high melting temperature (T_m) and a high strength. A shish-kebab micromorphology, accounting for about 5% of the crystals, was assigned. Kalay and Bevis[6] provided experimental evidence for the presence of a shish-kebab morphology in injection-molded iPP. Guan et al.[7] and Chen and Shen[8] also considered that their experimental results were related to the production of shish-kebab crystals when they studied self-reinforced polymers by oscillating packing injection molding. Through the investigation of injection-molded iPP by means of small- and wide-angle X-ray scattering, Wenig and Herzog[9] drew the conclusion that the skin layer exhibits an oriented shish-kebab structure. With respect to the skin thickness of injection-molded iPP, Brenna and Soltfeldt-Ellinggsen[10] reported that the thickness was about 0.1 mm, and Fujiyama et al.[11] thought it was about 0.6 mm.

Trotignon and Verdu[12–14] reported that variations in the degree of crystallinity, macromolecular orientation, and β-phase fraction are related to a complex layered morphology for iPP moldings. As far as crystal forms in iPP moldings are concerned, it had been thought that the commercial grades of iPP crystallized predominantly in the α phase, with only a sporadic presence of the β phase formed at low crystallization temperatures.[15] However, Varga[16] proved that the β phase can occur in commercially processed iPP in large quantities. Moreover, Kalay and coworkers[6,17,18] presented evidence for the occurrence of the γ phase in commercially processed iPP, in addition to the α and β phases.

EXPERIMENTAL

Sample preparation

The iPP used in this study was the same as that described in the first article of this series,[1] J300 from Beijing Yanshan Petrochemical Co. (China). The samples tested were prepared by injection molding, for

Correspondence to: W. Dai (daiwenlp@xtu.edu.cn).

Journal of Applied Polymer Science, Vol. 88, 2791–2796 (2003)

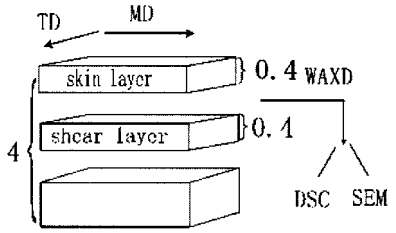

Figure 1 Schematic representation of the specimen preparation.

which the main molding parameters and the two-cavity mold employed were the same as those described in the first article.[1] A segment (15 mm × 10 mm × 4 mm) was taken along the machine direction (MD) from the center of the slab injection-molded, and then specimens from the surface to the core, about 0.4 mm thick, were sliced from the segment parallel to its surface, as shown in Figure 1. The specimens were designated as the skin and shear layer, respectively. These specimens were first used for X-ray diffraction experiments; some were sectioned into some small pieces for scanning electron microscopy (SEM), and some samples (10–12 mg) were used for differential scanning calorimetry (DSC). SIF skin and shear layer specimens are designated SIF skin and SIF shear, respectively, and conventional flow process (CFP) skin and shear layer specimens are designated CFP skin and CFP shear, respectively.

SEM

SEM (JEOL JSN-5600LV and s-520, Japan) was applied for the examination of the surfaces of the CFP and SIF samples. All the samples, except the impact fracture samples, were etched for different predetermined times with the permanganic etching technique.[19,20] The samples were sprayed with a very thin layer of gold before observations were made.

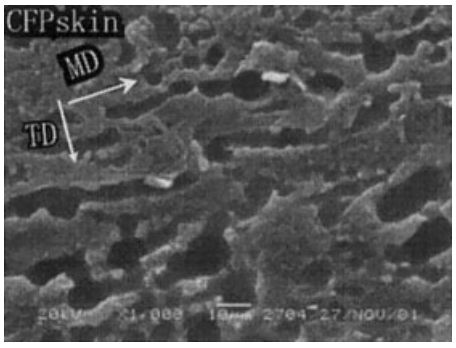

Figure 2 SEM micrograph of the etched surface from a CFP skin sample.

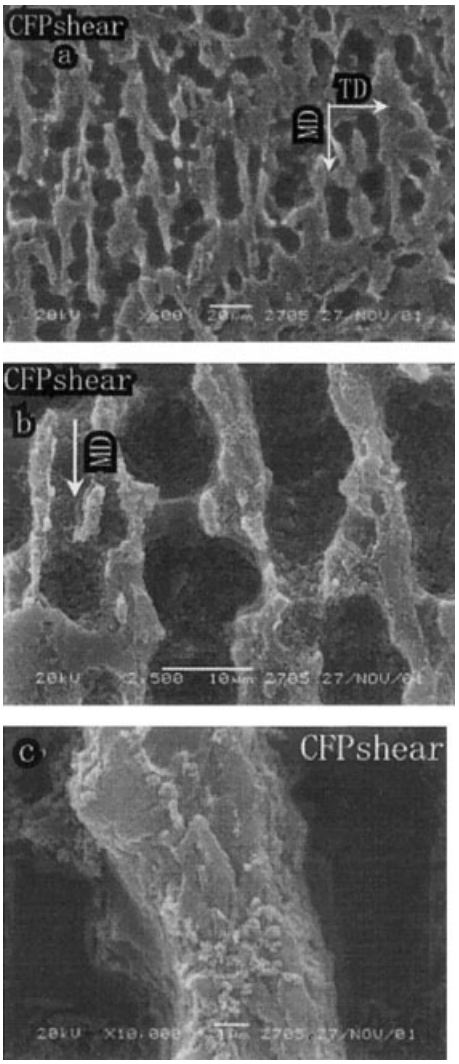

Figure 3 SEM micrographs of the etched surface from a CFP shear sample: (a) lower magnification, (b) local amplification, and (c) local high amplification.

Wide-angle X-ray diffraction (WAXD)

WAXD studies were carried out on the samples with a D/MAX-III A X-ray diffractometer (Japan). Diffraction curves were measured in the diffraction angle interval of $2\theta = 5–45°$. Cu Kα radiation was used, and monochromatization was achieved with a graphite monochromator. The crystallinities were obtained from the ratio of the areas under the crystalline peaks to the total area of the diffractograms. Additionally, β-phase indices were used to quantify the relative proportions of the β phase in light of the literature.[21]

DSC

A PerkinElmer DSC-7 (USA) was used for the measurements of DSC thermograms. The samples (10–12 mg) were cut from samples that had been used in the previous WAXD experiments. A heating rate of 10°C/

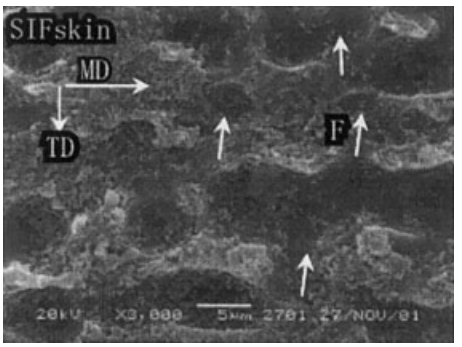

Figure 4 SEM micrograph of the etched surface from an SIF skin sample.

min was applied. The T_m's and crystallinities of the moldings were determined and used for the discussion on phase relations in iPP moldings. The heat of fusion (ΔH_m) for 100% crystalline iPP was taken to be 138 J/g.[22]

RESULTS AND DISCUSSION

SEM observations

SEM micrographs of CFP skin and CFP shear are displayed in Figures 2 and 3, respectively. These two figures show that the amorphous polymer etched out is strongly extended along the MD, that is, the melt flow direction, whereas the crystals are aligned along the MD for the intense shear flow, or the coaction of both elongational flow and shear flow. The small, round holes in these figures [clearer in Fig. 3(b)] result from the crystal grains etched out for the dissolution of the amorphous polymer on their surfaces. It is an interesting phenomenon that the holes or grains are preferentially aligned along the MD. The structure that these two figures describe reveals that there exists a flow of one dimension in the skin and shear layers during conventional injection molding. The tensile extent of the amorphous polymer is high, and the crystal length parallel to the MD is longer, as shown in Figure 3(c).

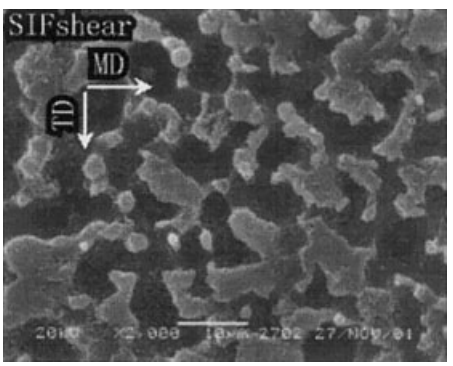

Figure 5 SEM micrograph of the etched surface from an SIF shear sample.

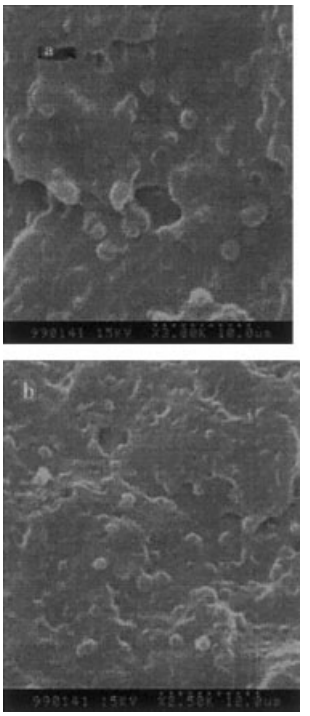

Figure 6 SEM micrographs of impact failure surfaces (s-520): (a) SIF sample and (b) CFP sample.

Figures 4 and 5 illustrate the microstructures of SIF skin and SIF shear, respectively. Figure 4 reveals that although the grains are aligned in the MD, some discontinuous parts, marked with F arrows, appear on or between the longer crystals parallel to the MD. This implies that there exists a flow in the transverse direction (TD), that is, a transverse flow. In the shear layer solidified through SIF, the amorphous and crystalline phases are randomly distributed, as shown in Figure 5. This texture is produced by the SIF of two dimensions. Comparing Figure 5 to Figure 3, one can determine that the microstructure of Figure 5 displays a

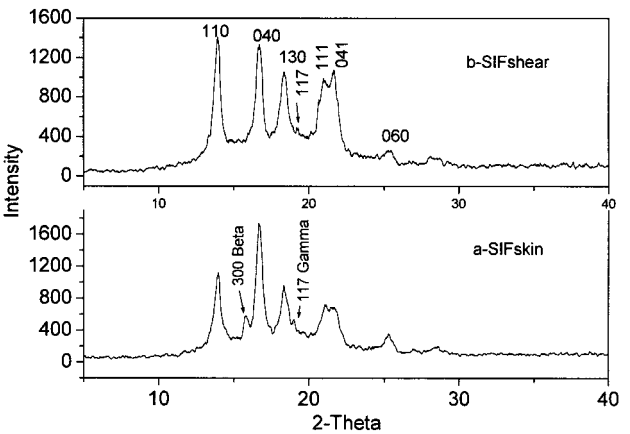

Figure 7 X-ray diffraction profiles from SIF samples.

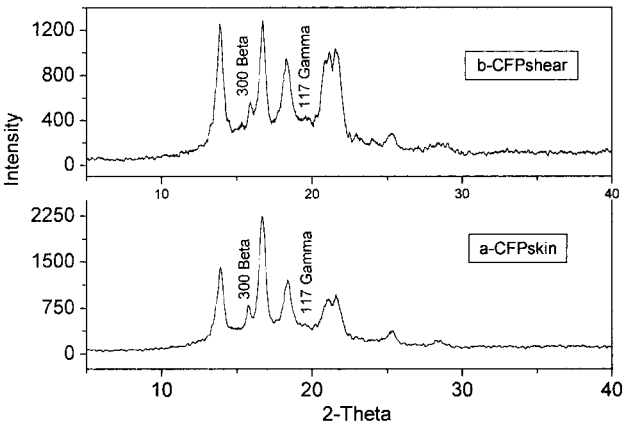

Figure 8 X-ray diffraction profiles from CFP samples.

better dispersion of the amorphous polymer in the moldings; alternatively, the oriented amorphous polymer occurs both in the MD and in the TD in large quantities. This is conducive to an increase in the impact strength. If the studies on shrinkage in the TD and the thickness distribution of the SIF samples in our previous article[1] are macroscopic evidence for the presence of the transverse flow, the SEM micrographs are microscopic evidence.

Figure 6(a,b) shows the impact failure surfaces of SIF and CFP samples. Many crystal grains in these two photographs can be observed. We regard the holes appearing in Figures 2–5 to be the results of the grains being etched out.

WAXD results

X-ray diffraction profiles from SIF skin and SIF shear are displayed in Figure 7(a,b), respectively, and those from CFP skin and CFP shear are shown in Figure 8(a,b). Some X-ray diffraction results, including the β-phase index, are reported in Table I. The results of the WAXD experiments indicate that the crystalline fraction in CFP and SIF skin samples contains α, β, and γ phases, whereas in SIF shear samples, the crystalline fraction does not contain the β phase, or the β-phase content is so small that it is not reflected in the curve. The β-phase content in skin layers is greater than that in shear layers. This is consistent with the conclusion that the tendency for β-phase formation in iPP injection moldings is high in the shear region[23] and at low T_m's.[9,18,24]

According to Table I, each layer for the SIF sample possesses a higher crystallinity than the corresponding layer of the CFP sample; the shear layers for the SIF sample and for the CFP sample exhibit a higher crystallinity, which is consistent with the results obtained by DSC.

TABLE I
Results of the X-Ray Diffraction Analysis

Sample	2θ (°)	Miller indices (*hkl*)	β-Phase index	X_c (%)[a]
SIF skin	13.960	110	0.106	47.31
	16.727	040		
	18.380	130		
SIF shear	13.947	110	~0	52.03
	16.727	040		
	18.384	130		
CFP skin	13.962	110	0.113	46.92
	16.737	040		
	18.408	130		
CFP shear	13.938	110	0.086	49.16
	16.762	040		
	18.381	130		

[a] Crystallinity.

TABLE II
Results of the DSC Studies

Sample	T_m (°C)	T_{sm} (°C)	ΔH_m (J/g)	X_c (%)[a]
SIF skin	165.00	114.06, 142.01, 151.07, 158.07	77.04	55.8
SIF shear	166.78	114.75	86.65	62.80
CFP skin	165.90	113.78, 142.30, 151.07	76.27	55.27
CFP shear	165.42	114.15	78.87	57.15

[a] Crystallinity.

DSC results

We performed DSC experiments to compare the occurrences of different phases and crystallinities in samples due to different flowing conditions in the cavity. The T_m values, the melting temperatures of any crystal form appearing as secondary peaks (T_{sm}'s), and the crystallinities of the samples tested are tabulated in Table II. The crystallinity of each layer of the SIF samples is greater than that of the corresponding layer of the CFP samples, and this agrees with what was previously drawn with the X-ray diffraction method.

Figures 9 and 10 show the DSC thermograms ob-

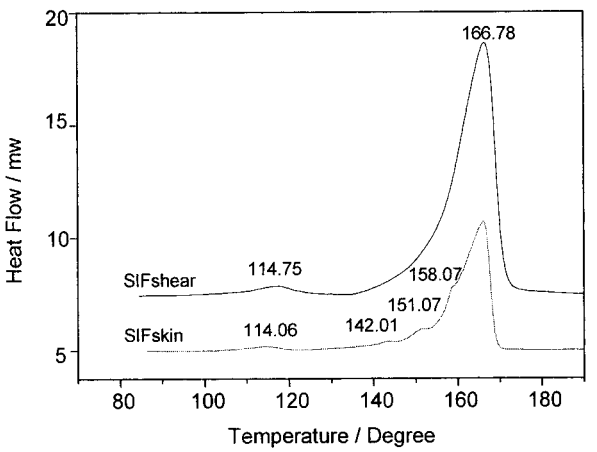

Figure 9 DSC thermograms for SIF samples.

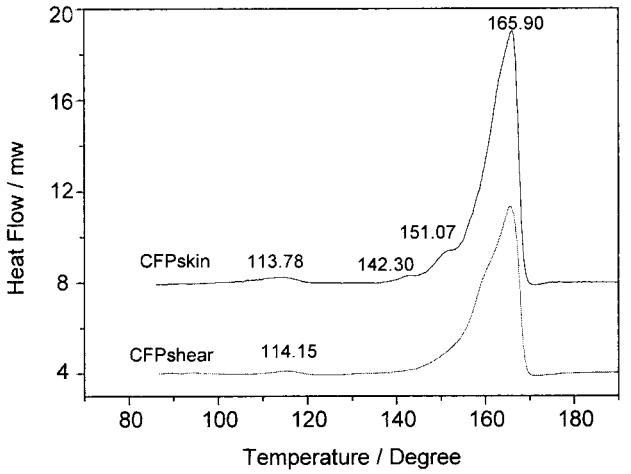

Figure 10 DSC thermograms for CFP samples.

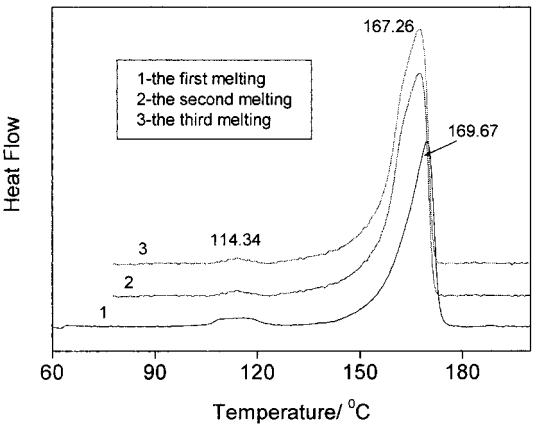

Figure 11 DSC thermograms for original iPP: (1) the first melting, (2) the second melting, and (3) the third melting.

tained from the SIF and CFP samples, respectively. All the thermograms show a main melting peak at about 165°C for all the samples tested. Varga[25,26] and Fillon et al.[27] reported that the β phase, crystallized above the lower critical temperature limit (~105°C), melts around 150°C, depending on the exact crystallization temperature. According to this conclusion and the analysis carried out by Kalay and Bevis,[6] T_{sm}'s around 142 and 150°C for the SIF skin and CFP skin samples correspond to the melting of the β phase, and T_{sm} around 158°C for the SIF skin sample also corresponds to the melting of the β phase.

We notice that the DSC curves for the SIF skin and CFP skin samples show the secondary peaks of the β phase but for the SIF shear and CFP shear samples show no peak. This indicates that the crystalline portion in the SIF skin and CFP skin samples contains a higher β-phase content but in the SIF shear and CFP shear samples contains a smaller β-phase content. This result is consistent with that obtained by the X-ray diffraction method. The β phase in the CFP shear sample in reality exhibits an endotherm around 158°C, which is overlapped by the α-phase endotherm, as displayed in Figure 10.

All the samples in Figures 9 and 10 exhibit an endotherm around 114°C. Marigo et al.[28] reported that the DSC thermogram for an ethylene–propylene copolymer containing 100% γ phase showed a single endotherm with a maximum at 119°C. At first, we thought that the endotherms around 114°C corresponded to the melting of the γ phase. To further explain the endotherm around 114°C, we used an original iPP sample for DSC experiments. Figure 11 shows the continuous thrice melting curves, and Figure 12 shows the continuous twice cooling curves. During the thrice melting processes, all the curves exhibit an endotherm around 114°C (see Fig. 11), and during the cooling processes, both curves exhibit an exothermic peak at about 95°C. Therefore, the endotherm around 114°C may be caused by the composition of the polymer used (e.g., its molecular chain structure) and addition agents.

CONCLUSIONS

This article has examined the effects of two different flowing models in the cavity, SIF and CFP, on the morphology and crystallinity of iPP moldings. The conclusions of this research can be summarized as follows:

1. SIF of the melt in the cavity during injection molding, which is different from CFP, results in a transverse flow. This transverse flow weakens the shear action in the direction parallel to the MD and strengthens the action in the direction perpendicular to the MD.
2. The dispersion of amorphous iPP in SIF samples is better than that in CFP samples for the occurrence of the oriented amorphous polymer both in

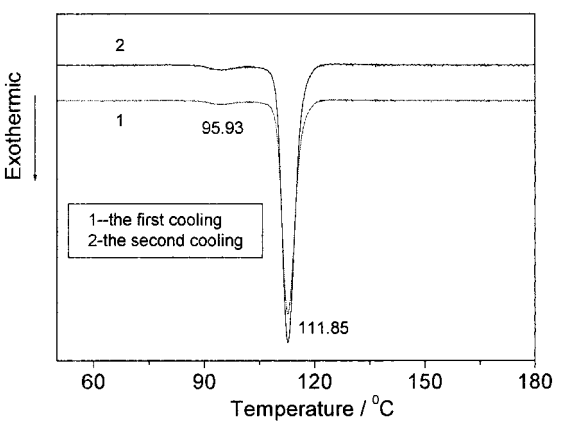

Figure 12 Cooling curves for original iPP: (1) the first cooling and (2) the second cooling.

the MD and in the TD, and this is brought about by the transverse flow.

3. SIF samples exhibit a higher crystallinity than CFP samples. The γ phase occurs in iPP injection moldings, in addition to α and β phases. This is consistent with the conclusion drawn by Kalay and Bevis.[6] DSC thermograms can show the endotherm of the γ phase.

References

1. Wenli, D.; Pengsheng, L.; Xiayu, W. J Appl Polym Sci 2003.
2. Kantz, M. R. Int J Polym Mater 1974, 3, 1753.
3. Kantz, M. R.; Newman, H. D.; Stigale, F. H. J Appl Polym Sci 1972, 16, 1249.
4. Katti, S. S.; Schultz, J. M. Polym Eng Sci 1982, 22, 1001.
5. Fujiyama, M.; Wakino, T. J Appl Polym Sci 1988, 35, 29.
6. Kalay, G.; Bevis, M. J. J Polym Sci Part B: Polym Phys 1997, 35, 265.
7. Guan, Q.; Zhu, X.; Shen, K. J Appl Polym Sci 1996, 62, 755.
8. Chen, L. M.; Shen, K. J Appl Polym Sci 2000, 78, 1911.
9. Wenig, W.; Herzog, F. J Appl Polym Sci 1993, 50, 2163.
10. Brenna, A.; Soltfeldt-Ellinggsen, D. Morphology of Polymer; de Gruyter: Berlin, 1986; p 271.
11. Fujiyama, M.; Masada, I.; Mitani, K. J Appl Polym Sci 2000, 78, 1571.
12. Trotignon, J. P.; Verdu, J. J Appl Polym Sci 1987, 34, 1.
13. Trotignon, J. P.; Verdu, J. J Appl Polym Sci 1987, 34, 19.
14. Trotignon, J. P.; Verdu, J. J Appl Polym Sci 1990, 39, 1215.
15. Padden, F. J.; Keith, H. D. J Appl Phys 1959, 30, 1479.
16. Varga, J. J Therm Anal 1989, 35, 1891.
17. Kalay, G.; Allan, P.; Bevis, M. J. Polymer 1994, 35, 2480.
18. Kalay, G.; Allan, P.; Bevis, M. J. Plast Rubber Compos Process Appl 1995, 23, 71.
19. Olley, R. H.; Hodge, A. M.; Bassett, D. C. J Polym Sci Polym Phys Ed 1979, 17, 627.
20. Olley, R. H.; Bassett, D. C. Polymer 1982, 23, 1707.
21. Raab, M.; Kotek, J.; Baldrian, J.; Grellmann, W. J Appl Polym Sci 1998, 69, 2255.
22. Fatou, J. G. Eur Polym J 1971, 7, 1057.
23. Dragaun, H.; Hubeny, H.; Muschik, H. J Polym Sci Polym Phys Ed 1977, 15, 1779.
24. Fleischmann, E.; Zipper, P.; Janosi, A.; Geymayer, W.; Koppelman, J.; Schurz, J. Polym Eng Sci 1989, 29, 835.
25. Varga, J. J Therm Anal 1986, 31, 165.
26. Varga, J. J Therm Anal 1989, 35, 1891.
27. Fillon, B.; Thierry, A.; Wittmann, J. C.; Lotz, B. J Polym Sci Part B: Polym Phys 1993, 31, 1407.
28. Marigo, A.; Marega, C.; Zannetti, R.; et al. Makromol Chem 1989, 190, 2805.